CrystEngComm

ROYAL SOCIETY OF CHEMISTRY

PAPER

View Article Online
View Journal | View Issue

Cite this: *CrystEngComm*, 2020, **22**, 8110

A novel one-pot strategy to rapidly synthesize bright red emitting upconversion nanocrystals with core–shell–shell structure†

Zhiyuan Cheng, [a] Hao Lin,[b] Tong Liu,[a] Yongjin Li, [a] Shenghong Yang[a] and Yueli Zhang*[a]

Received 10th September 2020,
Accepted 15th October 2020

DOI: 10.1039/d0ce01320j

rsc.li/crystengcomm

β-$NaErF_4$:0.005Tm upconversion nanocrystals (UCNCs) with core–shell structure are quite popular due to efficient red upconversion luminescence. However, the traditional seed-mediated growth method is not continuous and quite time consuming, while the successive layer-by-layer strategy is unfriendly because of the usage of toxic sodium trifluoroacetate (Na-TFA). In this work, we utilized a novel one-pot strategy to synthesize β-$NaErF_4$:0.005Tm with core–shell–shell structure. The morphology of the core could be significantly regulated. $NaYbF_4$ and $NaYF_4$ shells could be epitaxially grown on the core by simply adding fresh raw materials and heating to 300 °C, successively. Thanks to the suppression of surface quenching and energy back transfer from Yb^{3+} to Er^{3+}, the population density of excited states of Er^{3+} ($^4I_{13/2}$, $^4I_{11/2}$ and $^4I_{9/2}$) was much improved, resulting in the tremendously enhanced upconversion intensity of β-$NaErF_4$:0.005Tm@$NaYbF_4$@$NaYF_4$. This one-pot protocol could supply core–shell–shell red UCNCs with regular morphology, enhanced intensity and long-lasting decay lifetime, offering promising opportunities for applications such as bioprobing, anti-counterfeiting, photodynamic therapy, *etc.*

1. Introduction

Upconversion nanoparticles (UCNCs) activated by rare earth (RE) ions have been explored widely thanks to their unique properties such as large anti-Stokes shift, line emission, low toxicity, real intermediate level, and long lasting lifetime, and promising applications like sensing, detecting, bioimaging, photodynamic therapy, anti-counterfeiting, magnetic resonance imaging (MRI),[1–14] *etc.*

Among all the UCNCs, β-$NaErF_4$ is a promising candidate because it can be pumped using an 808/980/1532 nm laser and can emit red and green photons.[15] However, its potential was limited by its poor efficiency. In 2017, Liu[16] found out that slightly doped Tm^{3+} ions could act as energy trapping centers and significantly enhanced the upconversion luminescence (UCL). Thereafter, β-$NaErF_4$:0.005Tm became well-known red emitting UCNCs, many researches followed up and now it is clear that β-$NaErF_4$:0.005Tm has great potential for versatile applications. For example, Mei[17] utilized β-$NaErF_4$:Tm,Yb as core and realized dumbbell shaped core–shell UCNCs with switchable upconversion under different excitation wavelengths; these UCNCs were then used for programmable activation of two ion channels, VChR1 and Jaws, for the purpose of membrane polarization. Li[18] conjugated β-$NaErF_4$@$NaLuF_4$ with commercial photosensitizer Ce6 and applied the nanophotosensitizers for photodynamic therapy and multimode imaging. Wang[19] reported that the 1525 nm emission of β-$NaErF_4$@$NaLuF_4$ could be much enhanced by doping 20% Yb^{3+} in the core. After coating with PAA, the UCNCs were used for short wave infrared imaging of cells and tissues and brain vasculature.

Despite so many works on β-$NaErF_4$:0.005Tm, the core–shell UCNCs were usually synthesized by only two traditional strategies: the seed-mediated growth method and successive layer-by-layer strategy. The seed-mediated growth method[20–22] required no toxic substances (*e.g.* Na-TFA), but wasted plenty of time on repetitive washing, centrifuging and degassing because the synthesis of the core and shell is not continuous. The successive layer-by-layer strategy[23–25] realized continuously synthesis of the shell but was not user-friendly because toxic Na-TFA must be used as shell precursor. Few studies concentrated on improving methods for rapid one-pot synthesis. Chen[26] proposed a facile time-saving and effective solid–liquid-thermal-decomposition (SLTD) method to form β-$NaReF_4$ (Re = Sm, Eu, Gd, Tb, Y) nanocrystals. It was significant to realize the synthesis of β-$NaErF_4$:0.005Tm

[a] *State Key Laboratory of Optoelectronic Materials and Technologies, School of Materials Science and Engineering, Sun Yat-Sen University, Guangzhou, 510275, China. E-mail: stszyl@mail.sysu.edu.cn*
[b] *School of Physics and Materials Science, Guangzhou University/The Research Center for Advanced Information Materials, Huangpu Research & Graduate School of Guangzhou University, Guangzhou 510006, China*

† Electronic supplementary information (ESI) available. See DOI: 10.1039/d0ce01320j

by this fast SLTD method because of the unique excellent upconversion properties of β-$NaErF_4$:0.005Tm.

In this work, we developed this SLTD method and synthesized β-$NaErF_4$:0.005Tm successfully. The influence of different experimental conditions on the morphology of the core was studied. β-$NaErF_4$:0.005Tm@$NaYbF_4$, β-$NaErF_4$:0.005Tm@$NaYF_4$ and β-$NaErF_4$:0.005Tm@$NaYbF_4$@$NaYF_4$ with core–shell structure were also synthesized in one pot. The core–shell structure of β-$NaErF_4$:0.005Tm@$NaYbF_4$@$NaYF_4$ was proved by TEM images. The UCL intensity was tremendously enhanced and the upconversion enhancement mechanism was proposed.

2. Experimental

2.1 Chemicals

$RECl_3{\cdot}6H_2O$ (RE = Y, Tm, Yb) (99.99%), $ErCl{\cdot}6H_2O$ (99.5%), sodium acetate (NaAc) (A.R. 98%), oleic acid (OA) (A.R. 85%), 1-octadecene (1-ODE) (A.R. 90%) and cyclohexane (99.5%) were purchased from Aladdin. $NaHF_2$ (A.R. 98%) was purchased from Macklin. All materials were used without further purification.

2.2 Synthesis of shell precursors Yb–OA and Y–OA

Before synthesizing UCNCs, the shell precursors Yb–OA and Y–OA were synthesized. In a typical experiment, 10 mmol $RECl_3{\cdot}6H_2O$ (RE = Y, Yb) was mixed with 40 mL OA and 60 mL 1-ODE in a 250 mL three-neck round-bottom flask. After degassing for 10 min to remove oxygen, the mixture was heated to 160 °C under N_2 flow with constant stirring to completely dissolve $RECl_3{\cdot}6H_2O$, then cooled down to room temperature (RT) naturally. The obtained RE–OA solution was then stored in a 100 ml bottle.

2.3 Synthesis of α-$NaErF_4$:0.005Tm UCNCs

The synthesis of α-$NaErF_4$:0.005Tm UCNCs named A0 could be described as follows: a stoichiometric amount of $RECl_3{\cdot}6H_2O$, 10 ml OA and 15 ml 1-ODE was added into a 100 ml three-neck round-bottom flask successively. After degassing for 10 min to remove oxygen, the resulting mixture was heated to 160 °C under N_2 flow with constant stirring for 30 min, then cooled down to RT. Thereafter, a stoichiometric amount of $NaHF_2$ and NaAc was added, and the solution was heated and kept at 250 °C for 30 min, then cooled down to RT. All of the obtained solutions were transferred into two centrifuge tubes and precipitated by the addition of ethanol. The precipitate was collected after centrifugation and washed with cyclohexane and ethanol 3 times, and re-dispersed in cyclohexane for further characterization.

2.4 Synthesis of hexagonal core-only UCNCs

All core-only UCNCs could be synthesized by similar procedures. As an example, sample B3 could be obtained by the following process: 1.5 mmol $RECl_3{\cdot}6H_2O$, 10 ml OA and 15 ml 1-ODE were added into a 100 ml three-neck round-bottom flask successively. After degassing for 10 min to remove oxygen, the resulting mixture was heated to 160 °C under N_2 flow with constant stirring for 30 min, then cooled down to RT. Thereafter, a stoichiometric amount of $NaHF_2$ and NaAc was added, and the solution was heated and kept at 250 °C for 30 min and 300 °C for 90 min under N_2 flow successively, then cooled down to RT. 10 ml of the obtained solution was transferred into two centrifuge tubes and precipitated by the addition of ethanol. The precipitate was collected after centrifugation and washed with cyclohexane and ethanol 3 times, and re-dispersed in cyclohexane for further characterization.

2.5 Synthesis of hexagonal core–shell UCNCs

All core–shell UCNCs could be synthesized by similar procedures. As an example, β-$NaErF_4$:0.005Tm@$NaYbF_4$@$NaYF_4$ CSS (core–shell–shell) UCNCs were synthesized by a modified process. β-$NaErF_4$:0.005Tm (core UCNCs) was first synthesized by the procedure mentioned above. Then, the middle absorption shell ($NaYbF_4$) was grown on the core. A stoichiometric amount of Yb–OA and $NaHF_2$ and 4 ml OA and 6 ml 1-ODE were added successively. After degassing for 10 min to remove oxygen, the resulting mixture was heated and kept at 250 °C for 30 min and 300 °C for 90 min under N_2 flow successively, then cooled down to RT. 10 ml of the obtained solution was transferred into two centrifuge tubes and precipitated by the addition of ethanol. The precipitate was collected after centrifugation and washed with cyclohexane and ethanol 3 times, and re-dispersed in cyclohexane for further characterization. The outer inert shell ($NaYF_4$) was grown last. A stoichiometric amount of Y–OA and $NaHF_2$ and 4 ml OA and 6 ml 1-ODE was added successively. After degassing for 10 min to remove oxygen, the resulting mixture was heated and kept at 250 °C for 30 min and 300 °C for 90 min under N_2 flow successively, then cooled down to RT. All of the obtained solution was transferred into two centrifuge tubes and precipitated by the addition of ethanol. The precipitate was collected after centrifugation and washed with cyclohexane and ethanol 3 times, and re-dispersed in cyclohexane for further characterization. β-$NaErF_4$:0.005Tm@$NaYbF_4$ and β-$NaErF_4$:0.005Tm@$NaYF_4$ were synthesized by similar procedures and named CAS (core–absorption shell) and CIS (core–inert shell) UCNCs, respectively.

2.6 Characterization

Powder X-ray diffraction (XRD) patterns of all the samples were recorded using a Rigaku X-ray diffractometer (Smartlab, Cu Kα radiation). TEM images were taken using an FEI transmission electron microscope (TEM, Tecnai G2 Spirit, 120 keV). High-angle annular dark field (HAADF) images and elemental linescans were obtained using an FEI TEM (FEI Tecnai G2 F30, 300 keV). Luminescence spectra and lifetime decay curves were measured using an Edinburgh Instruments setup (FLS 980) with 980 nm and 1532 nm diode lasers.

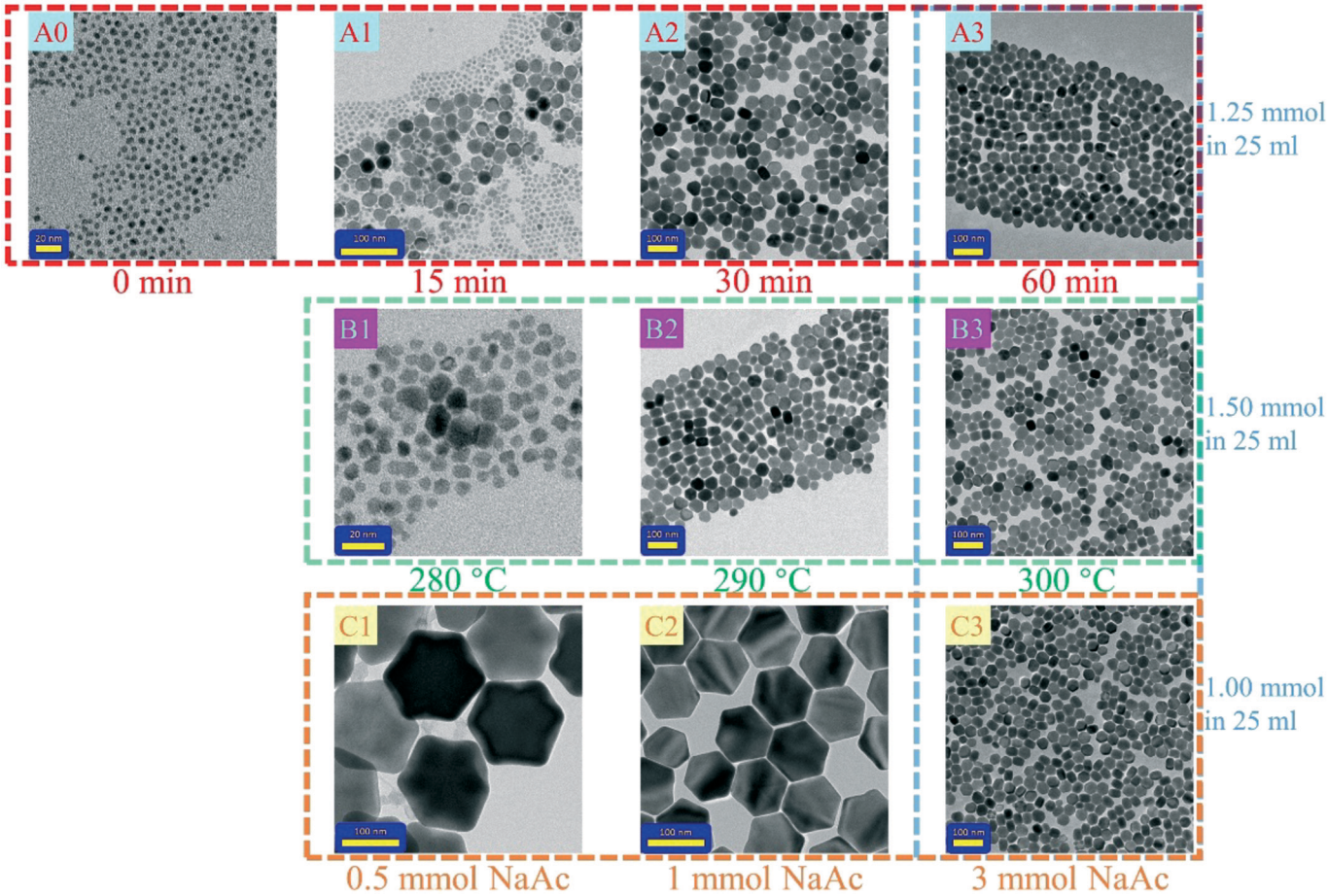

Fig. 1 TEM images of the UCNCs prepared under different experimental conditions. The variables of A0–A3, B1–B3, C1–C3 and A3–C3 were the synthesis duration, synthesis temperature, addition of NaAc and the molar weight of RE–OA and $NaHF_2$, respectively. The scale bars of A0 and B1 were 20 nm and the others were 100 nm.

3. Results and discussion

3.1 Structure and morphology

To obtain core-only β-$NaErF_4$:0.005Tm with uniform morphology, multiple experimental conditions were optimized and their influence on the crystal structure and morphology was investigated thoroughly. The variation of morphology with synthesis duration is shown in Fig. 1A0–A3. Sample A0, heated to 250 °C for 30 min, only contained small irregular nanoparticles, in which the phase was confirmed to be cubic (α-phase) by XRD as shown in Fig. 2. Sample A1, kept at 300 °C for 15 min, consisted of both hexagonal nanosheets with a size of about 20 nm and irregular nanoparticles. Meanwhile, the synthesis duration was extended to 30 min, sample A2 only contained hexagonal nanosheets with a heterogeneous size. For sample A3 heated for 60 min, only hexagonal nanosheets with a better size distribution were observed. Hence, the nanocrystal growth mechanism could be inferred as the Ostwald ripening process: the α-phase was stable at a lower temperature (250 °C), but when the synthesis temperature was raised up to 300 °C, the α-phase became unstable, favoring the transition from α to β-phase, and the crystal seeds of the β-phase formed. As a consequence, the seeds of the β-phase grew into nanosheets at the cost of α-phase irregular nanoparticles.

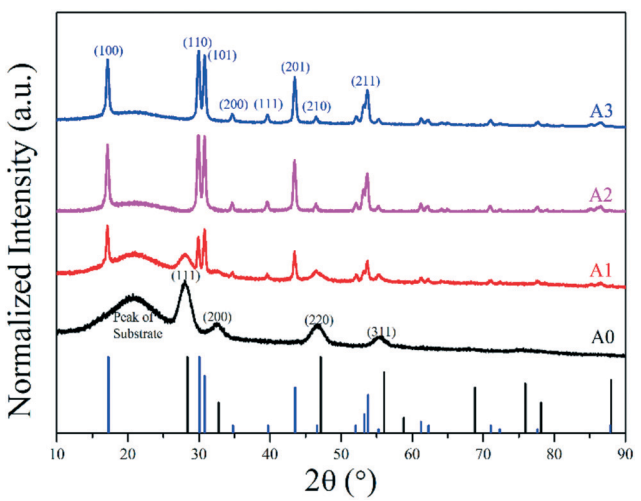

Fig. 2 XRD patterns of samples A0–A3, and the reaction duration at 300 °C of which was 0, 15, 30, and 60 min, respectively. The black vertical line was the standard XRD pattern of the α phase (PDF no. 27-0688) and the blue one was that of the β phase (PDF no. 27-0689).

The phase transition temperature was also confirmed. As shown in Fig. 1B1–B3 and S1,† while the synthesis duration was fixed at 60 min, the temperature was varied from 280 to 300 °C. The samples synthesized at 290 and 300 °C were pure hexagonal phases, while at 280 °C, they were mostly cubic phases, suggesting that 290 °C is the lowest temperature to complete the transition from the cubic phase to the hexagonal phase.

It has been proposed that the Na/RE ratio could influence the size of the final products. As the Na/RE ratio increased, the formation of β-phase seeds was favored, leading to the reduction of the size of the final products.[26] In our case, as shown in Fig. 1 C1–C3, when adding 0.5–3 mmol NaAc into the flask, the average size of the as-synthesized samples remarkably decreased from ~150 to 38.3 nm, which was consistent with the above theory. However, the size distribution of sample A3 was still diverging, which was not friendly for the subsequent epitaxial growth of a homogeneous shell. Surprisingly, we found that raising the molar weight of RE–OA and $NaHF_2$ could overcome this drawback. As shown in Fig. 1 and S2,† when the molar weight of RE–OA and $NaHF_2$ increased from 1 and 2 mmol to 1.5 and 3 mmol, respectively, the standard deviation significantly decreased from 6.44 (C3) to 3.75 (B3), suggesting that the distribution was significantly restrained. Besides, the average size slightly decreased from 38.3 nm (C3) to 35.0 nm (B3) too. Our results suggested that the molar weight of all the raw materials, including NaAc, $NaHF_2$ and RE–OA, was a non-negligible factor influencing the size distribution of the final core samples.

Core-only UCNCs, especially UCNCs with nanometer size, suffered severe surface quenching due to their big specific surface area. The most effective strategy to avoid the surface quenching phenomenon was the epitaxial growth of an inert shell to cut off the energy transfer (ET) from the active/sensitive ions to the surface quenching centers.[16] Further, coating an absorption layer was also beneficial for the upconversion luminescence (UCL) intensity by improving the absorption cross section; hence, it was really important to realize convenient, rapid, user-friendly and one-pot synthesis of UCNCs with core–shell structure. In our previous work, we proved that inserting $NaYbF_4$ shell between β-$NaErF_4$:0.005Tm and inert shell could obviously enhance the UCL intensity. For the purpose of intensity enhancement, we carried out the one-pot synthesis of β-$NaErF_4$:0.005Tm (core), β-$NaErF_4$:0.005Tm@$NaYF_4$ (CIS), β-$NaErF_4$:0.005Tm@$NaYbF_4$ (CAS) and β-$NaErF_4$:0.005Tm@$NaYbF_4$@$NaYF_4$ (CSS) and their TEM images were shown in Fig. 3. The sample core and the cores of CIS, CAS and CSS were synthesized by the same method; the molar weights of the shells of CIS and CAS and the middle shell of CSS were consistent with half of the molar weight of outer shell of CSS. It could be seen that as the shell

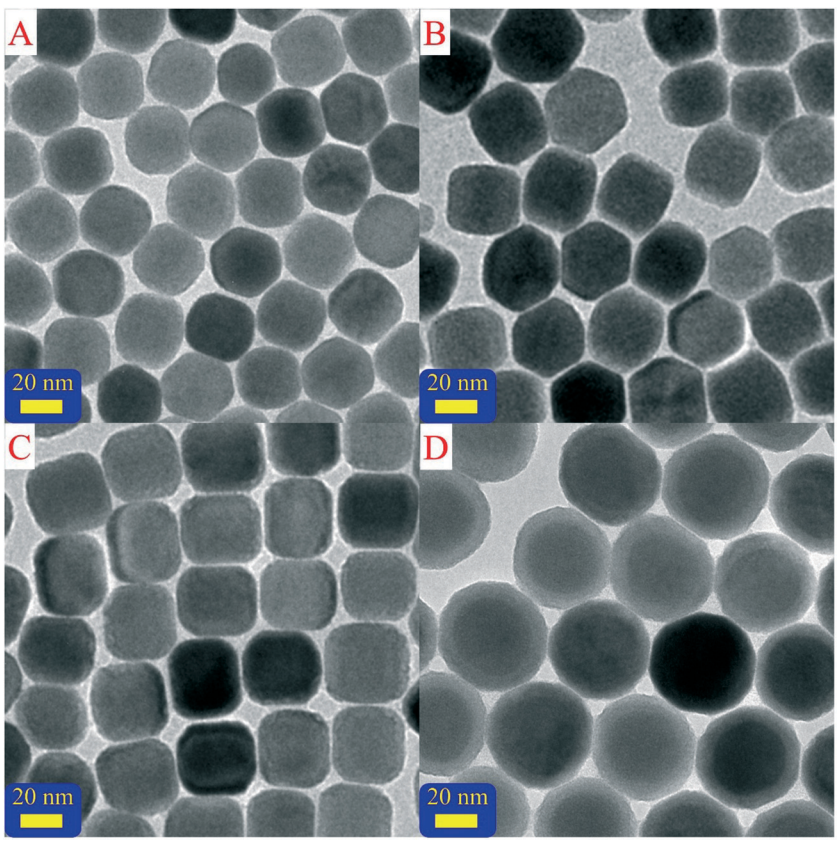

Fig. 3 TEM images of β-$NaErF_4$:0.005Tm (core), β-$NaErF_4$:0.005Tm@$NaYF_4$ (CIS), β-$NaErF_4$:0.005Tm@$NaYbF_4$ (CAS) and β-$NaErF_4$:0.005Tm@$NaYbF_4$@$NaYF_4$ (CSS) labeled as A–D, respectively. The scale bars were 20 nm.

was coated on the core, the samples were clearly enlarged. As shown in Table S1,† the average sizes of the core, CIS, CAS and CSS were 31.0, 35.8, 35.5 and 48.6 nm, respectively. The outer $NaYF_4$ shell could be easily distinguished from the core and middle shell by its lower grey value because the ability of Y^{3+} to scatter electrons is weaker than that of Er^{3+} and Yb^{3+}. Additional evidence for the core–shell–shell structure was the elemental linescans and elemental mapping of sample CSS, as shown in Fig. S3 and S4.† The signals of Er^{3+} and Yb^{3+} ions were majorly distributed in the core and core–shell areas, respectively; meanwhile, the signals of Y^{3+} ions were majorly distributed in the outer shell area. These results indicated that all the RE^{3+} ions were well confined in the pre-designed layers.

3.2 Upconversion luminescence (UCL) and mechanisms

The upconversion luminescence (UCL) of β-$NaErF_4$:0.005Tm is really important for its applications. Thanks to the abundant substates of Er^{3+} ions, β-$NaErF_4$:0.005Tm could be efficiently excited with both 980 and 1532 nm lasers, corresponding to the $^4I_{11/2}$ and $^4I_{13/2}$ states with an ideal absorption cross section, respectively. Fig. 4 showed the UCL spectra and decay lifetime curves of the samples core, CAS, CIS and CSS excited with 980 and 1532 nm lasers, respectively. In Fig. 4a and c, it could be seen that the spectra were mainly distributed in the red region peaking at 654 nm corresponding to the electron transition $^4F_{9/2} \rightarrow {}^4I_{15/2}$. The weaker emissions at the green region (520/540 nm, $^2H_{11/2}/{}^4S_{3/2} \rightarrow {}^4I_{15/2}$) and the weakest emissions at the near infrared (NIR) region (808 nm, $^4I_{9/2} \rightarrow {}^4I_{15/2}$) were observed too. The red to green ratio (R/G) of CSS was about 24.6 and 9.18 under 980 and 1532 nm lasers, respectively. The UCL intensities of core, CAS and CIS were much weaker than that of CSS under both 980 and 1532 nm lasers as listed in Table S2.† Compared with β-$NaErF_4$:0.005Tm (core), the intensity of CSS could be 291/17 366 folds enhanced when pumped with either the 980 nm laser or the 1532 nm laser. The outer $NaYF_4$ shell could suppress the surface quenching effect, *i.e.* the energy transfer

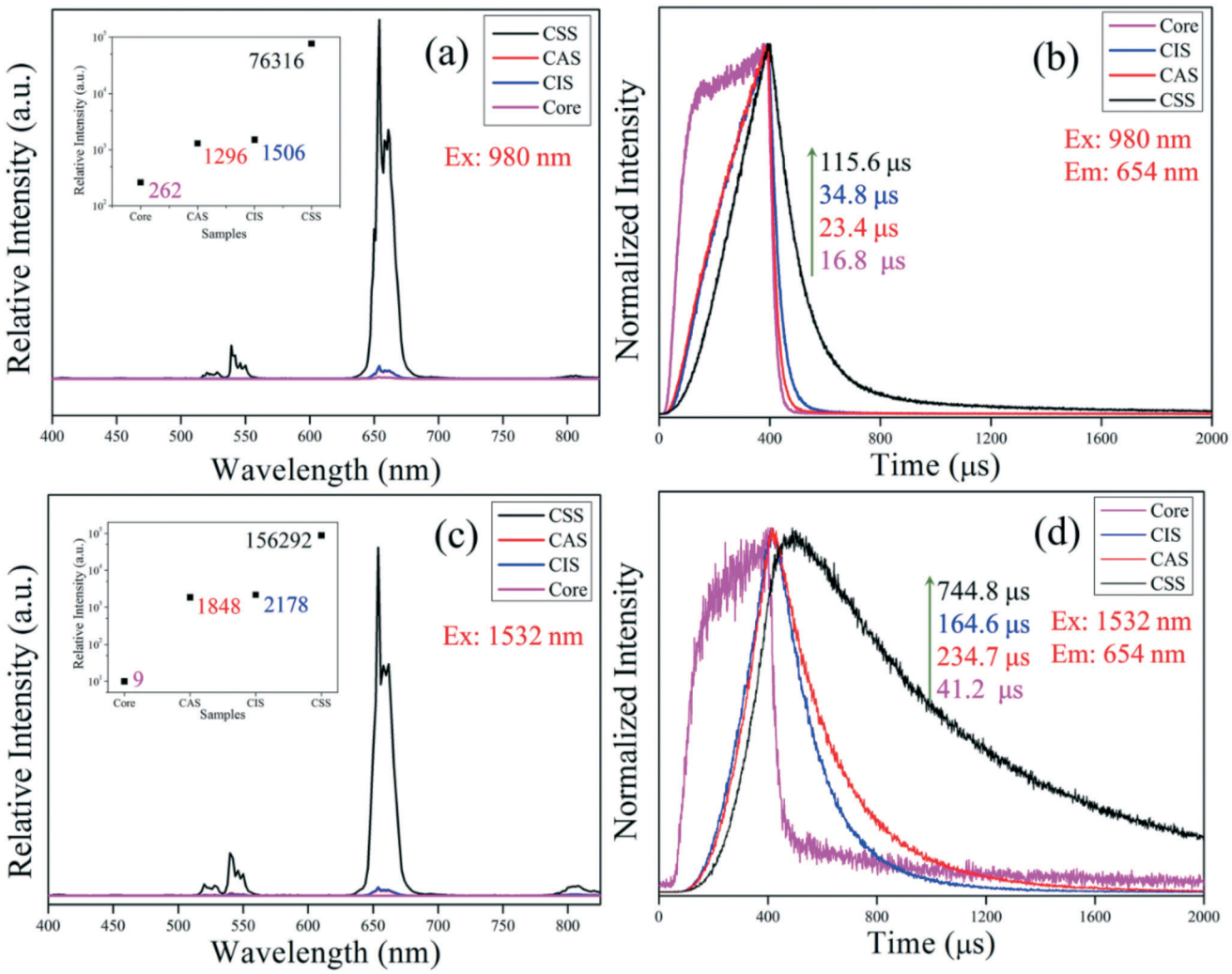

Fig. 4 The upconversion luminescence (UCL) spectra (a and c) and decay lifetime curves (b and d) of β-$NaErF_4$:0.005Tm (core), β-$NaErF_4$:0.005Tm@$NaYbF_4$ (CAS), β-$NaErF_4$:0.005Tm @$NaYF_4$ (CIS) and β-$NaErF_4$:0.005Tm@$NaYbF_4$@$NaYF_4$ (CSS). The laser power density was 10 W cm^{-2}.

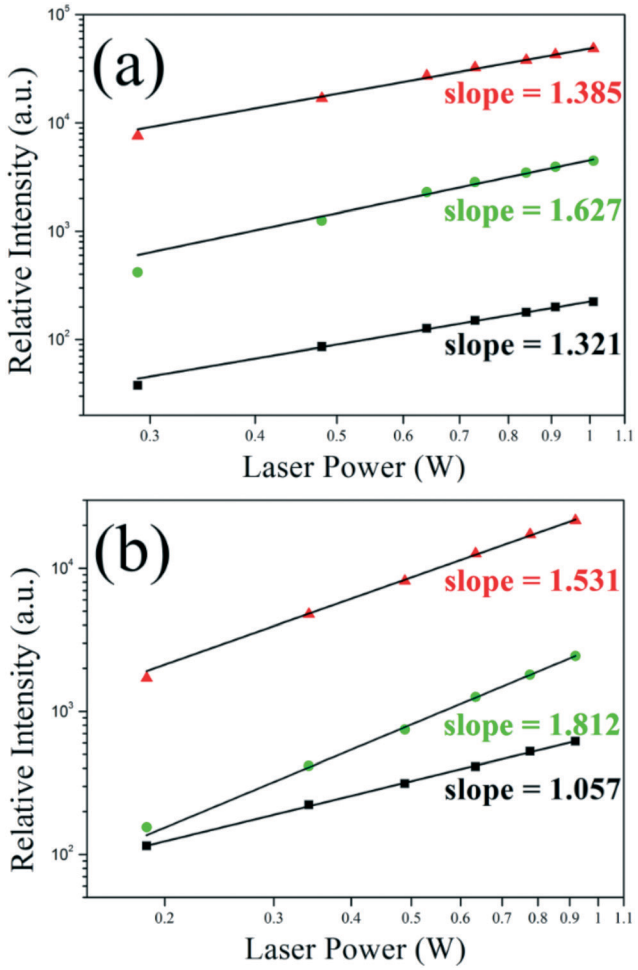

Fig. 5 The double logarithmic relationship of the NIR (808 nm), red (654 nm) and green (540 nm) UCL intensities *versus* the laser powers of the sample CSS pumped with 980 nm (a) and 1532 nm (b) lasers, respectively.

(ET) from active/sensitive ions to surface defects or ligands. When the inert shell stopped the leakage of energy, the population density of the excited states of the Er^{3+} ions ($^4I_{13/2}$, $^4I_{11/2}$, $^4I_{9/2}$, $^4F_{9/2}$, $^4S_{3/2}$, and $^2H_{11/2}$) raised and the UCL intensity was largely increased. As shown in Fig. 4b and d, the lifetimes of core, CAS, CIS and CSS were 16.8, 23.4, 34.8 and 115.6 μs, respectively, when excited with the 980 nm laser, and 42.1, 234.7, 164.6 and 744.8 μs, respectively, when excited with the 1532 nm laser. This was direct evidence for the shielding effects of outer $NaYF_4$. When the ET from activators to surface quenching centers was cut off, the UCL efficiency increased and the lifetime was prolonged. What's more, the population density of the lower states of Er^{3+} ($^4I_{13/2}$, $^4I_{11/2}$ and $^4I_{9/2}$) would also be enlarged by the suppression of surface quenching. Influenced by the enlarged population density of the lower states, the decay lifetime of $^4F_{9/2}$ (upper states) was prolonged too.

Fig. 5 and S5† displayed the double logarithmic relationship of the UCL intensity *versus* laser power and the upconversion luminescence spectra of the sample CSS, respectively. It could be seen that when pumped by the 980 nm laser, the slopes of the red, green and NIR peaks were 1.385, 1.627 and 1.321, slightly deviated from the theoretical value (n = 2), suggesting that only the first excited state ($^4I_{13/2}$) was partly saturated. However, when pumped by the 1532 nm laser, the slope of the red, green and NIR peaks was only 1.531, 1.812 and 1.057, respectively. It was well-known that the UCL from Er^{3+}@$^4F_{9/2}$ or $^4S_{3/2}$/$^2H_{11/2}$ was a three-photon process and the UCL from Er^{3+}@$^4I_{9/2}$ was a two-photon process when pumped with the 1532 nm laser; hence, these experimental values greatly deviated from the theoretical value. The sound reason for this deviation was the complete saturation of $^4I_{13/2}$ and the partial saturation of $^4I_{11/2}$ and $^4I_{9/2}$ of Er^{3+}.[27–29] This deduction could be supported by the lifetime curves. As indicated in Fig. 4d, when the 1532 nm laser shut down at 0.4 ms, unlike other samples or pumped with the 980 nm laser, the emission intensity of CSS not only didn't decline immediately, but also increased to the max value of about 0.1 ms later. That was to say, after 0.4 ms excitation with the 1532 nm laser, the population density of

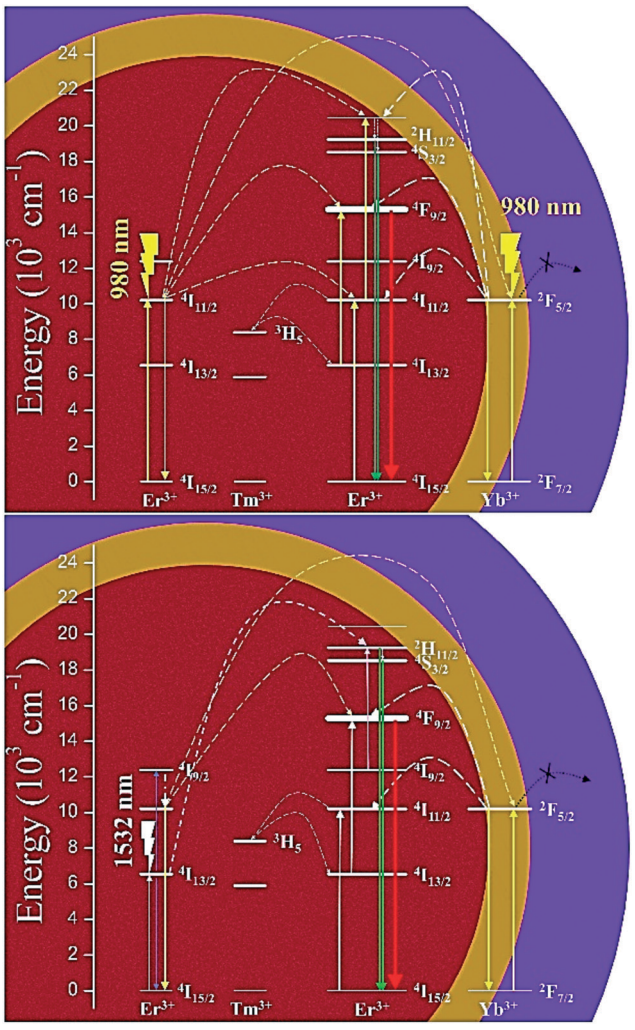

Fig. 6 The proposed energy transfer mechanisms of β-$NaErF_4$:0.005Tm@$NaYbF_4$@$NaYF_4$ CSS UCNCs excited with 980 nm laser (top) and 1532 nm lasers (bottom), respectively.

$^4I_{13/2}$, $^4I_{11/2}$ and $^4I_{9/2}$ was large enough to enhance the UCL intensity without continuous pumping for ~0.1 ms. Besides, the lifetime was longer when they were excited with the 1532 nm laser compared with the 980 nm laser, indicating that the population density of $^4I_{13/2}$, $^4I_{11/2}$ and $^4I_{9/2}$ was larger when pumped with the 1532 nm laser. The lifetime decay curve of $^4I_{9/2}$ is also shown in Fig. S7.† As a comparison, the lifetime of $^4I_{9/2}$ pumped with the 1532 nm laser was slightly lower than that with the 980 nm laser, which should have originated from the more intense interaction $^4I_{9/2} + {}^4I_{13/2} \rightarrow {}^2H_{11/2} + {}^4I_{15/2}$ because the population density of $^4I_{13/2}$ was higher when pumped with the 1532 nm laser, which was also consistent with our deduction.

The UCL mechanism is briefly summarized and shown in Fig. 6. Both red and green UCLwere a two-photon process when pumped with the 980 nm laser, and a three-photon process when pumped with the 1532 nm laser. The outer $NaYF_4$ shell (purple area) cuts off the energy leakage and prevents the surface quenching effects. The Yb^{3+} ions in the middle $NaYbF_4$ shell (yellow area) could be excited by directly absorbing 980 nm photons or accepting energy from Er^{3+} in the core; thereafter, Yb^{3+}:$^2F_{5/2}$ transferred energy back to Er^{3+}:$^4I_{13/2}$ or $^4I_{11/2}$, causing Er^{3+}:$^4F_{9/2}$ or Er^{3+}:$^4S_{3/2}$/$^2H_{11/2}$ with high efficiency. The population densities of the lower excited states of Er^{3+} ($^4I_{13/2}$, $^4I_{11/2}$, and $^4I_{9/2}$) were largely boosted thanks to both the suppression of the surface quenching and energy back transfer from Yb^{3+} to Er^{3+}, resulting in the tremendous enhancement of the UCL intensity.

4. Conclusion

In summary, a successive one-pot strategy to synthesize β-$NaErF_4$:0.005Tm with core–multishell structure was presented. Different experimental conditions were varied to obtain core-only β-$NaErF_4$:0.005Tm with uniform morphology and suitable size for further shell growth. The nanocrystal growth process was confirmed to be Ostwald ripening. To coat outer shells, RE–OA precursors, $NaHF_2$ powders and fresh OA/1-ODE were added into the reaction flask and heated at 300 °C; no extra complex steps were needed. What's more, this method could be used to coat multiple shells successively. The middle $NaYbF_4$ layer could transfer energy back to Er^{3+} in the core, and the $NaYF_4$ layer cuts off the energy transfer from the sensitizer/activator to surface quenching centers. Thanks to these effects, the population density of the excited states of Er^{3+} ($^4I_{13/2}$, $^4I_{11/2}$, and $^4I_{9/2}$) was partly or completely saturated, resulting in the tremendous enhancement of upconversion luminescence (UCL) intensity. This UCL mechanism was supported by both lifetime decay curves and double logarithmic relationship of the UCL intensity *versus* laser powers. These results suggested that our successive one-pot strategy was simple, controllable and time-saving to synthesize core–shell–shell β-$NaErF_4$:0.005Tm@$NaYbF_4$@$NaYF_4$ with much enhanced red UCL, making it suitable for versatile applications such as bioprobing, anti-counterfeiting, and photodynamic therapy.

Conflicts of interest

There are no conflicts of interest to declare.

Acknowledgements

This work was supported by the National Natural Science Foundation of China (No. 61975245), the Science and Technology Planning Project of Guangdong Province (No. 2017A010103035), a start-up foundation from Guangzhou University under Grant No. 69-18ZX10334, and the Youth Innovative Talents Project in Colleges and Universities in Guangdong Province under Grant No. 2018KQNCX193.

References

1 Z. M. Zhang, S. Shikha, J. L. Liu, J. Zhang, Q. S. Mei and Y. Zhang, *Anal. Chem.*, 2019, **91**, 548–568.
2 X. H. Zhu, J. Zhang, J. L. Liu and Y. Zhang, *Adv. Sci.*, 2019, **6**(22), 1901358.
3 L. D. Sun, Y. F. Wang and C. H. Yan, *Acc. Chem. Res.*, 2014, **47**(4), 1001–1009.
4 S. L. Gai, C. X. Li, P. P. Yang and J. Lin, *Chem. Rev.*, 2014, **114**(4), 2343–2389.
5 Y. Y. Liu, X. F. Meng and W. B. Bu, *Coord. Chem. Rev.*, 2019, **379**, 82–98.
6 J. J. Zhou, J. L. Leaño Jr., Z. Y. Liu, D. Y. Jin, K.-L. Wong, R.-S. Liu and J.-C. G. Bünzli, *Small*, 2018, **14**(40), 1801882.
7 H. H. Gorris and U. Resch-Genger, *Anal. Bioanal. Chem.*, 2017, **409**(25), 5875–5890.
8 J. Zhao, H. Q. Chu, Y. Zhao, Y. Lu and L. L. Li, *J. Am. Chem. Soc.*, 2019, **141**(17), 7056–7062.
9 M. Wang, J. Song, F. F. Zhou, A. R. Hoover, C. Murray, B. Q. Zhou, L. Wang, J. L. Qu and W. R. Chen, *Adv. Sci.*, 2019, **6**(10), 1802157.
10 H. Rabie, Y. X. Zhang, N. Pasquale, M. J. Lagos, P. E. Batson and K.-B. Lee, *Adv. Mater.*, 2019, **31**(14), 1806991.
11 Z. B. Luo, Q. G. Qi, L. J. Zhang, R. J. Zeng, L. S. Su and D. P. Tang, *Anal. Chem.*, 2019, **91**(6), 4149–4156.
12 Y. Q. Hu, Q. Y. Shao, X. Y. Deng, D. D. Song, S. Y. Han, Y. Dong and J. Q. Jiang, *J. Mater. Chem. C*, 2019, **7**, 11770–11775.
13 Q. Chen, C. Wang, L. Cheng, W. W. He, Z. P. Cheng and Z. Liu, *Biomaterials*, 2014, **35**(9), 2915–2923.
14 W. P. Fan, B. Shen, W. B. Bu, F. Chen, Q. J. He, K. L. Zhao, S. J. Zhang, L. P. Zhou, W. J. Peng, Q. F. Xiao, D. L. Ni, J. N. Liu and J. L. Shi, *Biomaterials*, 2014, **35**(32), 8992–9002.
15 H. Lin, D. K. Xu, Z. Y. Cheng, Y. J. Li and Y. L. Zhang, *Appl. Surf. Sci.*, 2020, **514**, 146074.
16 Q. S. Chen, X. J. Xie, B. L. Huang, L. L. Liang, S. Y. Han, Z. G. Yi, Y. Wang, Y. Li, D. Y. Fan, L. Huang and X. G. Liu, *Angew. Chem., Int. Ed.*, 2017, **56**(26), 7605–7609.
17 Q. S. Mei, A. Bansal, M. K. G. Jayakumar, Z. M. Zhang, J. Zhang, H. Huang, D. J. Yu, C. J. A. Ramachandra, D. J. Hausenloy, T. W. Soong and Y. Zhang, *Nat. Commun.*, 2019, **10**, 4416.
18 Q. Q. Li, X. D. Li, L. Zhang, J. Zuo, Y. L. Zhang, X. M. Liu, L. P. Tu, B. Xue, Y. L. Chang and X. G. Kong, *Nanoscale*, 2018, **10**, 12356–12363.

19 X. Wang, A. Yakovliev, T. Y. Ohulchanskyy, L. N. Wu, S. J. Zeng, X. J. Han, J. L. Qu and G. Y. Chen, *Adv. Opt. Mater.*, 2018, **6**(20), 1800690.
20 Z. Q. Li and Y. Zhang, An efficient and user-friendly method for the synthesis of hexagonal-phase $NaYF_4$:Yb/Er/Tm nanocrystals with controllable shape and upconversion fluorescence, *Nanotechnology*, 2008, **19**(34), 345606.
21 H. S. Qian and Y. Zhang, *Langmuir*, 2008, **24**(21), 12123–12125.
22 F. Wang, J. Wang and X. G. Liu, *Angew. Chem., Int. Ed.*, 2010, **49**(41), 7456–7460.
23 X. M. Li, D. K. Shen, J. P. Yang, C. Yao, R. C. Che, F. Zhang and D. Y. Zhao, *Chem. Mater.*, 2013, **25**(1), 106–112.
24 L. Lei, X. R. Dai, Y. Cheng, Y. S. Wang, Z. Xiao and S. Q. Xu, *J. Mater. Chem. C*, 2019, **7**, 3342–3350.
25 H. Lakhotiya, A. Nazir, S. Roesgaard, E. Eriksen, J. Christiansen, M. Bondesgaard, F. C. J. M. van Veggel, B. B. Iversen, P. Balling and B. Julsgaard, *ACS Appl. Mater. Interfaces*, 2019, **11**(1), 1209–1218.
26 W. W. You, D. T. Tu, W. Zheng, X. Y. Shang, X. R. Song, S. Y. Zhou, Y. Liu, R. F. Li and X. Y. Chen, *Nanoscale*, 2018, **10**, 11477–11484.
27 C. Homann, L. Krukewitt, F. Frenzel, B. Grauel, U. Resch-Genger and M. Haase, $NaYF_4$:Yb,Er/$NaYF_4$ core/shell nanocrystals with high upconversion luminescence quantum yield, *Angew. Chem., Int. Ed.*, 2018, **57**(28), 8765–8769.
28 U. Resch-Genger and H. H. Gorris, *Anal. Bioanal. Chem.*, 2017, **409**(25), 5855–5874.
29 C. Würth, M. Kaiser, S. Wilhelm, B. Grauel, T. Hirsch and U. Resch-Genger, *Nanoscale*, 2017, **9**, 4283–4294.